

Article

Investigation of Structural and Electronic Properties of $\text{CH}_3\text{NH}_3\text{PbI}_3$ Stabilized by Varying Concentrations of Poly(Methyl Methacrylate) (PMMA)

Celline Awino ^{1,2,*} , Victor Odari ^{2,3,*}, Thomas Dittrich ¹, Pongthep Prajontat ⁴, Thomas Sakwa ² and Bernd Rech ¹

¹ Helmholtz-Zentrum Berlin, Institut für Si-Photovoltaik, Kekuléstr. 5, D-12489 Berlin, Germany; dittrich@helmholtz-berlin.de (T.D.); bernd.rech@helmholtz-berlin.de (B.R.)

² Department of Physics, School of Natural Sciences, Masinde Muliro University of Science and Technology, P.O. Box 190-50100, Kakamega, Kenya; tsakwa@mmust.ac.ke

³ Department of Physics, School of Physical Sciences, University of Nairobi, P.O. Box 30197-00100, Nairobi, Kenya

⁴ Department of Materials Science, Faculty of Science, Kasetsart University, Bangkok 10900, Thailand; fscipop@ku.ac.th

* Correspondence: cawino@mmust.ac.ke (C.A.); vodari@mmust.ac.ke (V.O.); Tel.: +254-725-863-526 (C.A.); +254-723-927-357 (V.O.)

Received: 26 May 2017; Accepted: 18 July 2017; Published: 3 August 2017

Abstract: Studies have shown that perovskites have a high potential of outdoing silicon based solar cells in terms of solar energy conversion, but their rate of degradation is also high. This study reports on improvement on the stability of $\text{CH}_3\text{NH}_3\text{PbI}_3$ by passivating it with polymethylmethacrylate (PMMA). Structural and electronic properties of $\text{CH}_3\text{NH}_3\text{PbI}_3$ stabilized by polymethylmethacrylate (PMMA) were investigated by varying concentrations of PMMA in the polymer solutions. Stability tests were performed over a period of time using modulated surface photovoltage (SPV) spectroscopy, X-ray diffraction (XRD), and photoluminescence (PL) measurements. The XRD patterns confirm the tetragonal structure of the deposited $\text{CH}_3\text{NH}_3\text{PbI}_3$ for every concentration of PMMA. Furthermore, $\text{CH}_3\text{NH}_3\text{PbI}_3$ coated with 40 mg/mL of PMMA did not show any impurity phase even after storage in air for 43 days. The Tauc gap (E_{Tauc}) determined on the basis of the in-phase SPV spectra was found in the range from 1.585 to 1.62 eV for the samples stored during initial days, but shifted towards lower energies as the storage time increased. This can be proposed to be due to different chemical reactions between $\text{CH}_3\text{NH}_3\text{PbI}_3$ /PMMA interfaces and air. PL intensity increased with increasing concentration of PMMA except for the perovskite coated with 40 mg/mL of PMMA. PL quenching in the perovskite coated with 40 mg/mL of PMMA can be interpreted as fast electron transfer towards the substrate in the sample. This study shows that, with an optimum concentration of PMMA coating on $\text{CH}_3\text{NH}_3\text{PbI}_3$, the lifetime and hence stability on electrical and structural behavior of $\text{CH}_3\text{NH}_3\text{PbI}_3$ is improved.

Keywords: $\text{CH}_3\text{NH}_3\text{PbI}_3$; PMMA; surface photovoltage

1. Introduction

Hybrid organic inorganic perovskite (HOIP), for example, methylammonium lead triiodide ($\text{CH}_3\text{NH}_3\text{PbI}_3$) possesses several properties such as high absorption coefficient [1], long carrier diffusion length [2], ambipolar charge transport [3], high mobility [4], as well as the ability to be solution processed via a low temperature deposition method. The low temperature processing approach is useful for energy conservation and can be adopted for large-scale production and in

flexible devices [5]. Spin coating technique is considered as one of the widely used and cheapest techniques for film production method [6], however, it is difficult to realize uniform and homogenous film through spin coating process. Homogenous film formation is very crucial for high performance of the device since inhomogeneous film enhances recombination of charge carriers. Usually one-step solution process, two-step sequential method, and two-step interdiffusion are the most commonly used deposition approaches with spin coating techniques. Solar cells with the highest efficiencies were obtained using the one-step solution process [7]. The two-step process has also received considerable efficiencies—of about 15.7%—via low temperature processing [8], however there is a persistent problem of non-reproducibility due to incomplete reaction of lead iodide which reduces device performance.

Recently, several efforts have been made to enhance the stability of perovskite solar cells. For instance, Zhang et al. combined slow growth of perovskite film and introduced a ZnO interlayer and corresponding devices were highly reproducible with excellent stability [5]. Quan et al. used density functional theory (DFT) where the intercalation of phenylethylammonium between perovskites introduces van der Waals interactions with increased formation energies which improved device stability [9]. You et al. also reported on solution-processed perovskite solar cells with NiO_x and ZnO nanoparticles as hole and electron transporting layers with improved stability against water and moisture [10]. Moreover, introducing bromide into $\text{CH}_3\text{NH}_3\text{PbI}_3$ formed a mixed combination of $\text{CH}_3\text{NH}_3\text{PbI}_{3-x}\text{Br}_x$ with related devices having improved stability [11]. Other approaches introduced p-type polymers as protecting layers since the hydrophobicity of the polymers prohibit intrusion of moisture and water into perovskite heterojunction [12]. Among the polymers used to enhance stability of perovskite is polymethylmethacrylate (PMMA). PMMA is an amorphous, environmentally friendly, and cost effective polymer used in many applications, such as in making aircraft windows. Many researchers have reported on the passivating role of PMMA on perovskite by filling pinholes and surface traps [13–15]. Song et al. reported on the use of PMMA in passivating surface traps of electronic devices made of ZnO nanowires. Passivated ZnO nanowire FETs maintained their electrical properties under different environmental conditions while carrier concentration and mobility of un-passivated FETs were significantly influenced by the environmental [13].

Wang et al. reported on the stability and improved performance of perovskite solar cells by inserting a thin layer of PMMA between $\text{CH}_3\text{NH}_3\text{PbI}_3$ and Spiro-OmeTAD. They obtained power conversion efficiency of 18.1% with the cell maintaining less than 5% decrease in efficiency after 20 days [15]. The improved performance was due to reduced shunt paths between TiO_2 layer and Spiro-OmeTAD in which PMMA helped to fill the pinholes and grain boundaries in perovskite layer. Wang et al. also reported on the insulating tunnelling behavior of different polymers when inserted between perovskite and C60. The insulating polymer exhibited tunnelling behavior by suppressing charge recombination at contacts by selectively conducting one type of charge while blocking the other type of charge [16]. Luo et al. demonstrated high quality perovskite films employing PMMA as anti-solvent during spin coating process. PMMA was used to induce nucleation and growth of perovskite crystals [17].

In this article, we attempt to explore the possibility of improving the stability of perovskite layers by coating them with polymethylmethacrylate (PMMA). The interfacial interactions between perovskite and PMMA of different concentrations were studied. For long term stability, it is important to understand the interface interaction between perovskite/PMMA, so as to gain deeper understanding of the interactions between the two layers and how such interactions could influence electrical and structural properties for the development of stable perovskite based devices. It has been shown that incorporation of PMMA with carbon nanotubes could stabilize $\text{CH}_3\text{NH}_3\text{PbI}_3$ by inhibiting fast degradation [12]. Recently, Dittrich et al. reported on the temperature dependence of the band gap of $\text{CH}_3\text{NH}_3\text{PbI}_3$ stabilized with PMMA using SPV and observed a jump in the band gap at 40 °C corresponding to transition from the tetragonal to cubic phase. In contrast, there was no signature in the band gap for transition from the tetragonal to orthorombic phase and concluded that there were structural interactions between $\text{CH}_3\text{NH}_3\text{PbI}_3$ and PMMA interfaces [18]. Charge

transport properties and structural properties between perovskite and PMMA were investigated using modulated surface photovoltaic spectroscopy (SPV), photoluminescence (PL), and grazing incidence X-ray diffraction (GIXRD). GIXRD allows for the determination of phase structure from lattice planes that are perpendicular to the sample surface while SPV allows for characterization of electronic properties related to charge separation of photogenerated charge carriers, band gap, and defect states close to the band edge at the sample surface. Both GIXRD and SPV have the same order of information depth implying that penetration depth of GIXRD and transport length of photogenerated charge carriers are of the order of hundreds of nm [19]. Optical properties of perovskite layers have already been studied by photoluminescence (PL) measurements [20]. PL reveals optical transitions in perovskite films by through the process of radioactive recombination. However, PL spectroscopy requires a laser which can be challenging for its implementation. On the other hand, surface photovoltaic spectroscopy has been employed as a complimentary technique to photoluminescence since it gives information about charge separation of photogenerated electrons and holes due to illumination without radiative recombination processes [20]. SPV, as a technique, is surface sensitive and requires no contact for measurement of charge separation in semiconductor materials [21]. A modulated SPV signal can be obtained when absorption of incident light is followed by separation of charge carriers. Compared to other methods, modulated SPV spectroscopy can give information on onset energies, change of sign, defect states below the band gap [22], and can also be applied to measure diffusion length using the method developed by Goodmann [23]. Furthermore, SPV is very sensitive at low light intensities where charge separation takes place [18]. SPV can be used to study exponential defect states below the band gap of $\text{CH}_3\text{NH}_3\text{PbI}_3$ and previous studies showed that the addition of a small amount of ammoniumvaleric acid iodide (AVAI) into solution containing $\text{CH}_3\text{NH}_3\text{I}$ and PbCl_2 leads to a reduction in the value of defects below the band gap, and hence a reduction in the disorder in the material [24]. The study provides a better understanding of the electrical and structural behavior of $\text{CH}_3\text{NH}_3\text{PbI}_3$ coated with PMMA to promote development of stable related photovoltaic devices.

2. Materials and Methods

Molybdenum coated glass substrates ($23.5 \times 23.5 \text{ mm}^2$, PVcomB, Berlin, Germany) were sequentially cleaned using an ultrasonicator in detergent (Mucasol, Sigma-Aldrich, Schnelldorf, Germany), distilled water, acetone, and 2-propanol for 15 min each. For each step, nitrogen gas was used to dry the substrates. The cleaned substrates were immediately transferred and stored in a N_2 -filled glovebox in order to reduce water and O_2 adsorption on the substrate surface.

A 40 wt % perovskite precursor solution was prepared by dissolving methylammonium iodide ($\text{CH}_3\text{NH}_3\text{I}$, Dyesol, Queanbeyan, Australia) and PbCl_2 (Carl Roth, GmbH & Co. KG, Karlsruhe, Germany) with a molar ratio of 3:1 [25] in anhydrous N,N-dimethylformamide (DMF, Sigma Aldrich) and then stirred at 60°C overnight on a hotplate inside a nitrogen filled glovebox. Measurements of 0, 20, 40, and 80 mg of PMMA were each dissolved in 1 mL of butyl acetate and stirred on a hot plate at 60°C for 2 h in the glove box. Thin film samples were prepared by spin coating 100 μL of perovskite solution on molybdenum substrate using two-step spin coating parameters of 2000 rpm for 10 s and 3000 rpm for 30 s, followed by annealing on a hot plate at 100°C for 60 min in a nitrogen-filled glovebox. A warm solution of PMMA at 60°C (different concentrations in 1 mL of butyl acetate) [25] was immediately spin coated on top of annealed perovskite films at 2000 rpm for 60 s (see Figure 1). The perovskite samples coated with PMMA in different concentrations were stored in air and their behavior monitored over a period of 43 days. During this time, grazing incidence X-ray diffraction (GIXRD) and surface photovoltaic spectroscopy (SPV) measurements were performed on the samples. Whereas, PL measurements were only performed for as-prepared samples. GIXRD and SPV techniques confirmed that only optimum concentration of 40 mg/mL of PMMA coated on the Perovskite showed no impurity phase, even after staying in air for more than 43 days.

Modulated SPV spectra in the fixed capacitor arrangement [26] for standard measurements were performed in a spectral range between 0.4 and 4.0 eV for wide range and 1.4–1.8 eV for narrow range with a quartz prism monochromator (SPM2) and a halogen lamp. The wide range helps to determine the overview spectra of the SPV signals while the narrow range helps to determine onset energy, tail states, and approximate band gaps using Tauc plot [27]. The vacuum pressure was maintained at a base pressure of 2×10^{-6} mbar. A reference signal from the chopper with a modulated frequency of 8 Hz was fed into a lock in amplifier (EG & G 5210, princeton applied research, Oak Ridge, TN, USA). Lock in amplifier measured the signal from the sample as an x-signal (in-phase) and as a y-signal (phase shifted by 90°). Impedance buffer of high input resistance of about $50\text{ G}\Omega$ was used to match the measurement capacitor to the input resistance of the lock in amplifier. To monitor the stability of perovskite films coated with PMMA, SPV and GIXRD measurements were taken for the air stored samples on the day of preparation and after 43 days. The phase structure near the surface of perovskite films deposited on molybdenum substrate and coated with PMMA, kept in air for different days were investigated using grazing incidence X-ray diffraction (GIXRD, Brucker AXS D8 Advance, Karlsruhe, Germany) with Cu K α radiation using a step size of 0.02° and step time of 4 s. For photoluminescence (PL) measurements, a dye laser with an energy density of 1 mJ/cm^2 , pulse length of 5 ns, and a wavelength of 365 nm was used for pulsed excitation. The light was focused onto the sample and a lens collected emitted PL light from the sample. The PL intensity was measured for a wavelength range of 1100–400 nm using an avalanche photodiode with a preamplifier with a bandwidth of 15 MHz. The PL spectral dependent measurements were carried out by a quartz prism monochromator, which detected the signal at a time of 20 ns.

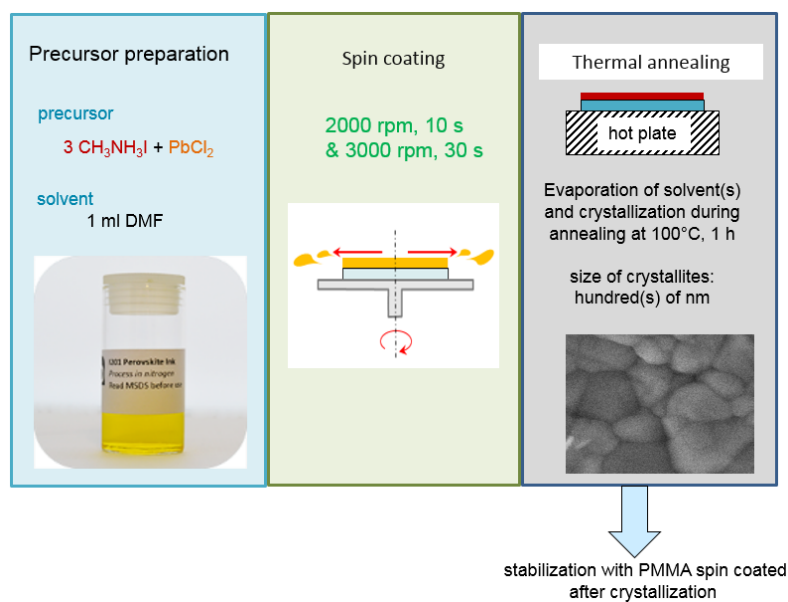


Figure 1. $\text{CH}_3\text{NH}_3\text{PbI}_3$ film preparation followed by PMMA capping layer.

3. Results and Discussion

Figure 2a shows in-phase and phase shifted by 90° SPV spectra for the sample deposited with 40 mg/mL PMMA onto the Mo substrate (i) and for Mo/ $\text{CH}_3\text{NH}_3\text{PbI}_3$ coated with PMMA at concentrations of 0, 20, 40 and 80 mg/mL (ii–v), respectively measured for as-prepared samples. For the sample in which only PMMA was deposited onto the substrate, there were no signals for both in-phase and phase shifted by 90°. This was attributed to the fact that PMMA is an insulator, hence no charge separation occurred. All perovskite samples showed a dominant onset of SPV signals at about 1.5 eV, i.e., at the bandgap of $\text{CH}_3\text{NH}_3\text{PbI}_3$ [28]. This correlates well with the existence of $\text{CH}_3\text{NH}_3\text{PbI}_3$ phase as revealed by the GIXRD measurements. When perovskite was coated with 0 mg/mL of

PMMA, in-phase signal was negative then changed sign, becoming positive at photon energy of 1.5 eV, reaches a maximum at 1.7 eV and again becomes negative at photon energies above 2 eV. This might be correlated to the presence of PbI_2 [21] as detected in the GIXRD measurements (see also Supplementary Information Figures S1 and S2). For perovskite coated with 20 mg/mL of PMMA, the in-phase signal was positive while the phase shifted by 90° signal was negative, indicating one mechanism of charge separation [24]. Positive in-phase signal has a maximum height of 0.51 mV at 1.7 eV and for the sample coated with 40 mg/mL of PMMA, both in-phase and phase shifted by 90° signals are positive, showing two mechanisms of charge separation. Photogenerated electrons were separated towards the Mo substrate while holes were preferentially separated towards external surface. The in-phase signal increased from 0.51 mV for 20 mg/mL of PMMA to 0.6 mV at 1.7 eV for 40 mg/mL PMMA. The increase in the value of in-phase signal correlates to the ongoing formation of $\text{CH}_3\text{NH}_3\text{PbI}_3$ as detected also with the increased GIXRD peak intensity for the same sample. For perovskite coated with 80 mg/mL of PMMA, the in-phase signal is positive while the phase shifted by 90° signal is negative, implying one mechanism of charge separation (i.e., opposite signs of the value of in-phase and phase shifted by 90° signals). The positive in-phase signal height of 0.41 mV has a maximum at 1.7 eV. The in-phase signal decreased from 0.6 mV for 40 mg/mL PMMA to 0.41 mV for 80 mg/mL PMMA. Irrespective of the concentration of PMMA, in-phase signals had a maximum photovoltage at photon energies of about 1.7 eV and onset energy of about 1.5 eV. This implies that increasing concentration of PMMA does not have an influence on the band gap of perovskite, indicating that it only acts as a protective layer on the surface of perovskite because of its excellent hydrophobic properties [12].

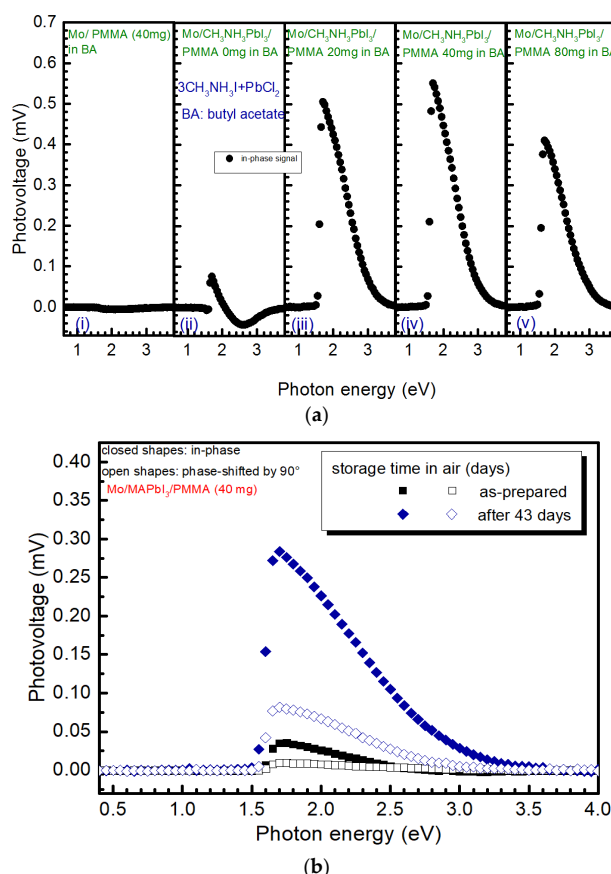


Figure 2. (a) Modulated in-phase (filled black symbols) for PMMA (40 mg/mL) deposited onto the Mo substrate (i) and for Mo/ $\text{CH}_3\text{NH}_3\text{PbI}_3$ coated with PMMA at concentrations of 0, 20, 40 and 80 mg/mL ((ii–v), respectively); (b) shows the overview spectra of the in-phase (filled symbols) and phase-shifted by 90° (open symbols) SPV spectra for as-prepared and after 43 days of storage in air for perovskite coated with PMMA at a concentration of 40 mg/mL.

Figure 2b shows the overview spectra of the in-phase and phase-shifted by 90° SPV signals measured for as-prepared sample and after 43 days of storage in air for perovskite coated with PMMA at a concentration of 40 mg/mL. A sharp onset between 1.5 and 1.6 eV was observed for all SPV spectra. During the whole period of measurement, no impure phase, such as PbI₂ phase, was detected.

Close to E_g for the as-prepared sample, and after 43 days of storage in air, both in-phase and phase-shifted by 90° signals were positive, indicating that photo-generated holes are preferentially separated towards the sample surface while electrons towards the bulk (substrate) [29]. Furthermore, the phase shifted by 90° signal was smaller in magnitude compared to in-phase signal. This suggests that trapping and de-trapping of charge carriers may lead to a slow response of the SPV spectra [18]. Since in-phase and phase shifted by 90° signals had the same signs, charge separation was caused by the two mechanisms of charge separation and that relaxation of SPV signals was due to recombination processes [24].

Figure 3 represents the GIXRD patterns of the Mo substrate coated with 40 mg/mL of PMMA and of CH₃NH₃PbI₃ deposited onto the Mo substrate and thereafter coated with PMMA at concentrations of 0, 20, 40 and 80 mg/mL for the as-deposited sample measured on the day of preparation. Not all samples showed PbI₂ peaks in the XRD patterns, and hence are good for studying the stability of CH₃NH₃PbI₃. PMMA was used as a blocking layer to prevent degradation of the perovskite film [30]. XRD shows the diffraction peaks at about 14.2°, 20.01°, 23.48°, 24.50°, 28.5°, 31.89°, 43.5°, and 59.0°, which were the characteristic tetragonal peaks of CH₃NH₃PbI₃. These diffraction peaks correspond to (110), (112), (211), (202), (220), (310), (314), and (440) planes of crystalline CH₃NH₃PbI₃, respectively. These results are in good agreement with the previous reports [19,31]. There are two dominant peaks at 14.2° and 28.5° in all the samples, indicating the formation of the crystalline perovskite. The peak intensity was relatively high for perovskite coated with PMMA at a concentration of 40 mg/mL. This implies that 40 mg/mL seems to be the optimum concentration of PMMA at which it acts as an efficient blocking layer for preventing the degradation of these CH₃NH₃PbI₃ films [30]. Since PMMA is an insulator, hydrophobic, and able to prevent the intrusion of moisture into the perovskite layer, concurrently inhibiting the evaporation of methylammonium iodide [12]. Small diffraction peaks at about 15.7° and 31.8° were also observed for all samples containing perovskite. These peaks could be correlated to the (100) and (200) diffraction peaks of CH₃NH₃PbCl₃ which is in agreement with previous reports [25]. It was interesting that the coating of PMMA on top of perovskite layer could significantly reduce the amount of CH₃NH₃PbCl₃ in the final perovskite films [29]. The peak at 40.47° appeared in all the samples even without perovskite. This could be supposed to be due to molybdenum substrate [31]. It was found that when using 80 mg/mL of PMMA, new peaks appeared at 35.80°, 39.50°, 47.70°, and 48.8°. The peak at 39.50° was identified to be a PbI₂ peak while remaining peaks were non-identified and their meanings have not yet been identified to the best of our knowledge. The appearance of the PbI₂ phase is correlated with the appearance of the SPV signal at about 2.3 eV [14,23].

After 43 days of storage in air (see Figure 4), impurity phase at 12.67° was observed for samples with 0 mg/mL and 20 mg/mL of PMMA coated on the perovskites. For perovskite coated with 80 mg/mL of PMMA, an impurity peak was observed at 39.50° with some extra peaks at 29.42°, 37.45°, and 45.74° corresponding to (200), (112), and (300) cubic phase of perovskite [32]. This implied that perovskite coated with 80mg/mL of PMMA coexisted in two phases (tetragonal and cubic phases) with continued storage in air. The impurity phases at 12.67° and 39.50° resembled those of PbI₂ and may be due to degradation of perovskite to its constituent precursor elements [25]. Perovskite coated with 40 mg/mL of PMMA did not show any impurity phase even after storage in air for 43 days. This indicates that 40 mg/mL of PMMA can be the optimum concentration for it to act as a blocking layer. However, for 80 mg/mL PMMA, small impurity phases at 12.67° and 39.50° were observed together with the coexistence of two phases.

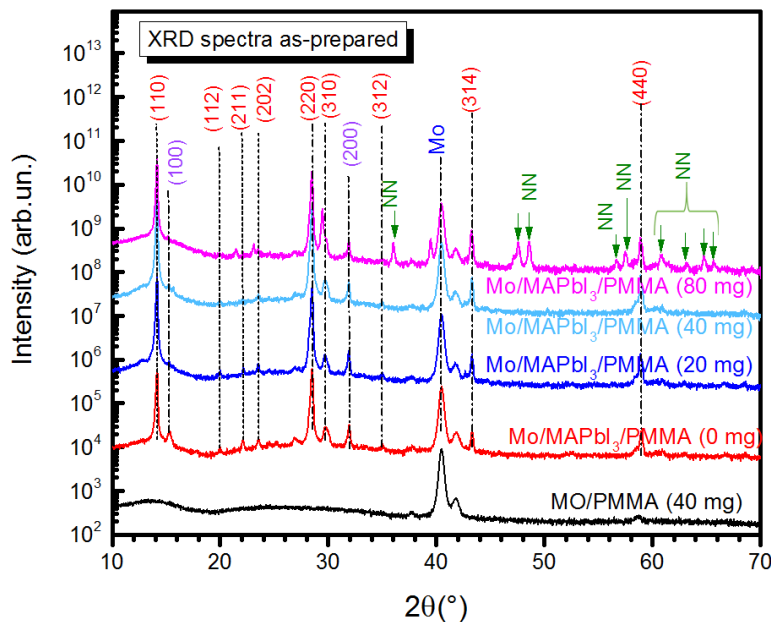


Figure 3. Grazing incidence X-ray diffraction patterns of Mo substrate coated with 40 mg/mL of PMMA (black); and of Mo/perovskite coated with PMMA at concentrations of 0, 20, 40, and 80 mg/mL (red, blue, dark cyan, and magenta, respectively) for the as-prepared sample.

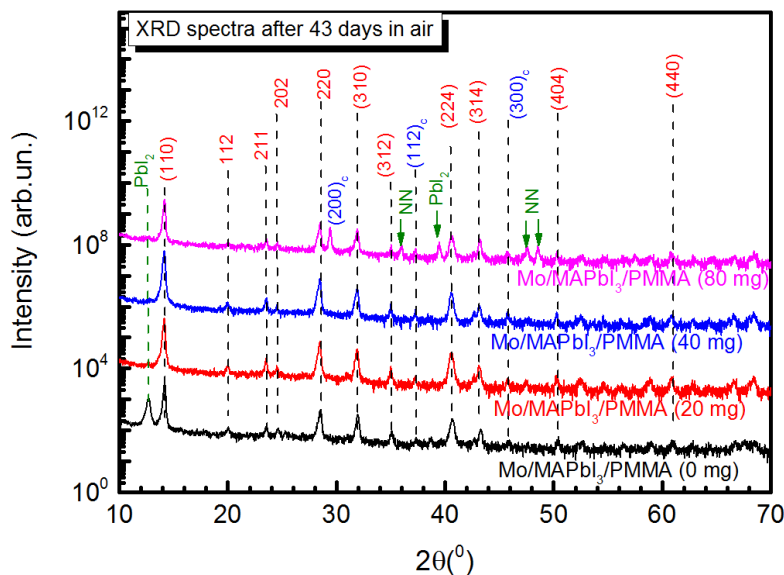


Figure 4. Grazing incidence X-ray diffraction patterns of Mo/perovskite coated with PMMA at concentrations of 0, 20, 40, and 80 mg/mL (black, red, blue, and magenta) after 43 days of storage in air.

Figure 5 shows PL spectra for perovskite coated with 0, 20, 40, and 80 mg/mL of PMMA and for 40 mg/mL PMMA on Mo substrate. The maximum emission was observed at the same wavelength of 775 nm for all perovskite samples. This was consistent with the data reported elsewhere [33] and corresponds to band gap of about 1.6 eV for tetragonal perovskite phase. For comparison, the Tauc gap obtained using SPV for the sample with 40 mg/mL of PMMA was 1.59 eV (see supporting information Figure S3). The PL intensity was increased with increasing concentration of PMMA except for 40 mg/mL, which was highly quenched, indicating radiative recombination process. Quenching in the sample with 40 mg/mL of PMMA might be attributed to fast electron transfer towards the substrate, which is in agreement with the SPV measurement in which both the in phase and phase shifted by 90°

signals were positive. The results also agree with the findings by Sun et al. [34]. There was no PL signal for 40 mg/mL PMMA on molybdenum substrate, since PMMA is an insulator [12] hence having no effect on PL spectrum. The band gap of perovskite did not change with concentration of PMMA, suggesting that PMMA only modifies the surface of $\text{CH}_3\text{NH}_3\text{PbI}_3$ without changing the bulk crystal.

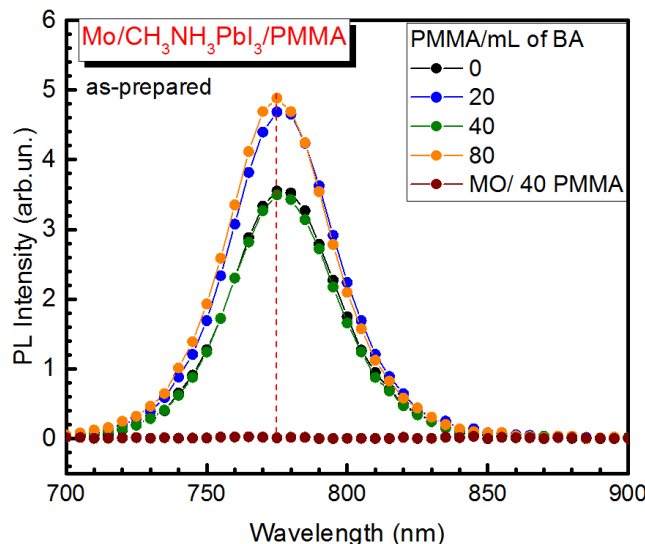


Figure 5. PL spectra for perovskite coated with 0, 20, 40, and 80 mg/mL of PMMA and for 40 mg/mL PMMA on Mo substrate.

Figure 6 shows maximum in-phase SPV signals on a logarithmic scale when the samples were stored in air for 43 days. Perovskite coated with 0 mg/mL of PMMA, a change of sign after the first day of storage in air was observed and an impurity phase of PbI_2 at around 2.3 eV [21] appeared as the storage time in air increased. This implied that perovskite degraded to PbI_2 with $\text{CH}_3\text{NH}_3\text{I}$ evaporating from the surface due to interaction with air and moisture [29]. This was also confirmed by the GIXRD spectrum that PbI_2 peak appeared at 12.67° [25] after exposure to air for more than one day. On the other hand, for perovskite coated with 20 mg/mL of PMMA, there was no change of sign, but the sample shows variability in the value of maximum in-phase signal. This implied that the sample was not stable and hence not suitable for studying stability test. Interestingly, perovskite coated with 40 mg/mL PMMA showed no change of sign in the value of in-phase signal, but showed a drop in the value of the in-phase signal on the second day by more than one order of magnitude. After the 2nd day until 18th day, the signal increased, before a slight drop was observed on the 43rd day of storage in air. The decrease of the signal might be due to degradation when the sample was exposed to air initially, thereafter with continued exposure to air there was passivation of surface defects. Finally, for perovskite coated with 80 mg/mL of PMMA, there was a change of sign on the 18th day of storage in air. The change of sign might be correlated to many processes contributing to charge separation, including the appearance of impurity phases.

Figure 7 shows a Tauc plot [27] as a function of storage time in air. E_{tauc} decreased monotonously with increasing storage time in air except for 80 mg/mL of PMMA, which showed a slight increase in band gap from 1.584 eV on first day to 1.589 eV on the 18th day of storage in air, before decreasing to 1.587 eV on the 43rd day of storage in air. The 20 mg/mL PMMA showed a wide band gap of more than 1.6 eV as compared to other samples during the first 18 days and smallest band gap of 1.55 eV after 43 days in air. Previous reports indicate that the band gap increases with the decrease in concentration [26] and this is in agreement with our findings on initial days in which 20 mg/mL of PMMA had the widest band gap while 80 mg had the narrowest band gap. In contrast, for 0 mg/mL, only solvent was used with no PMMA concentration. After 43 days in air, 20 mg/mL PMMA revealed the narrowest band gap, which might be due to impurity related defects. There is a shift in band gap

towards lower energies with an increase in storage time in air. This could be postulated to be due to different chemical and surface reactions between $\text{CH}_3\text{NH}_3\text{PbI}_3/\text{PMMA}$ interfaces with air.

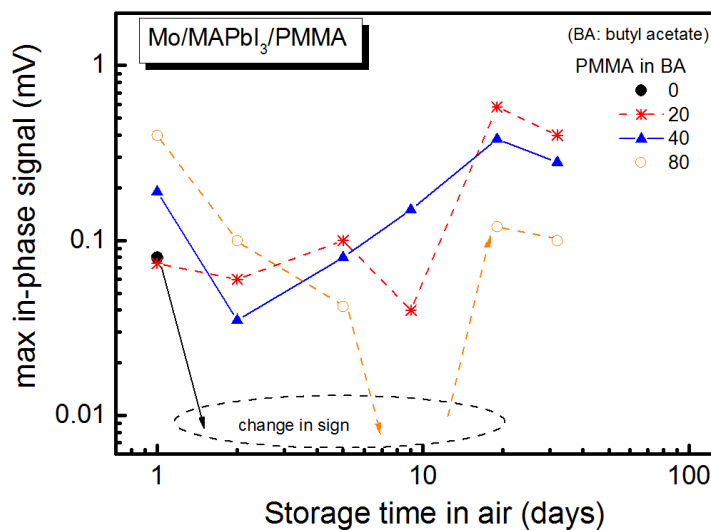


Figure 6. Maximum in-phase SPV spectra for the perovskite coated with PMMA at concentrations of 0, 20, 40, and 80 mg/mL stored in air on the 1st, 18th, and 43rd day.

Figure 8 shows the tail states of Mo/ $\text{CH}_3\text{NH}_3\text{PbI}_3/\text{PMMA}$ as a function of storage time in air. During the first day, the 0 mg/mL sample recorded the highest tail states of 45 meV. This might be attributed to intrusion of moisture related impurities into the film due to absence of PMMA that acts as a protective layer. Moreover, 20 mg/mL had a tail state of 42.5 meV which was still quite high as compared to 80 mg/mL with 26 meV. The 40 mg/mL sample had the least amount of tail states of about 18 meV which is comparable to an Urbach tail energy of 15 meV obtained by De Wolf et al. [1]. It was also observed that tail states decreased with continued storage in air and this can be attributed to increased surface defect passivation.

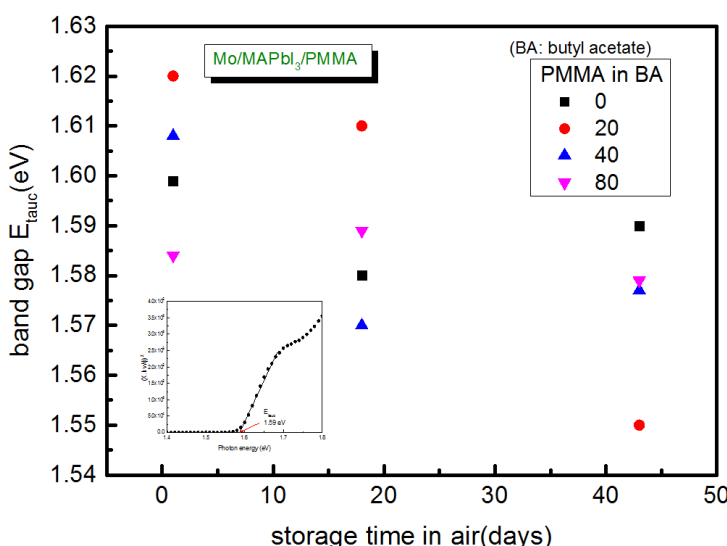


Figure 7. Band gap (E_{tauc}) for 0 mg/mL of (circle closed black rectangle), 20 mg/mL (closed red circle), 40 mg/mL (closed blue triangle), and 80 mg/mL (closed pink triangle) as a function of storage time in air on the 1st, 18th, and 43rd day. Inset shows Tauc plot for perovskite coated with 40 mg/mL of PMMA.

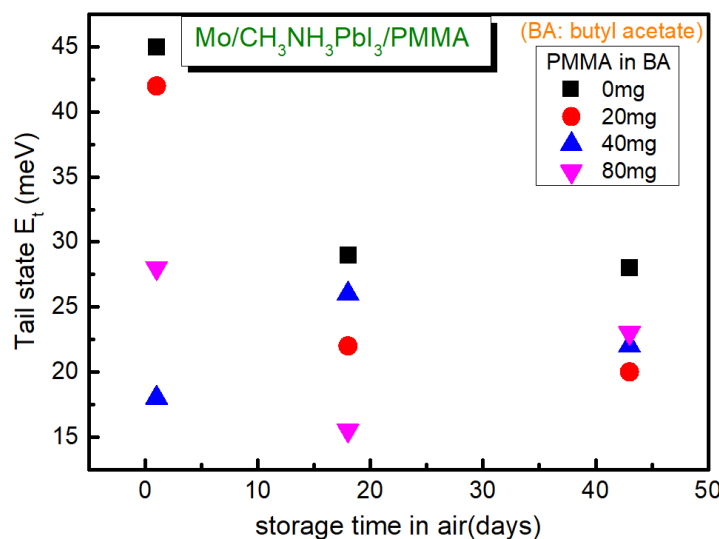


Figure 8. Tail states of Mo/ $\text{CH}_3\text{NH}_3\text{PbI}_3/\text{PMMA}$ with storage time in air for 0 (circle closed black rectangle), 20 (closed red circle), 40 (closed blue triangle), and 80 mg/mL of PMMA (closed pink triangle).

4. Conclusions

In conclusion, we successfully demonstrated that polymethylmethacrylate (PMMA) can be used to stabilize $\text{CH}_3\text{NH}_3\text{PbI}_3$ due to its hydrophilic nature which helps to inhibit intrusion of moisture into the perovskite layer. An optimum concentration of 40 mg/mL of PMMA coated on the Perovskite has no impurity phase, as confirmed by both GIXRD and SPV techniques, even after staying in air for more than 43 days. This was further confirmed by comparing the tail state of 18 meV obtained for perovskite coated with 40 mg/mL of PMMA with a reported Urbach energy tail of 15 meV. Stability testing also shows that there is a shift in the band gap towards lower energies with an increase in storage time and was attributed to different chemical and surface interactions at $\text{CH}_3\text{CH}_3\text{PbI}_3/\text{PMMA}$ interfaces. More studies as to the exact role of $\text{CH}_3\text{CH}_3\text{PbI}_3/\text{PMMA}$ interfaces for stabilization need to be further investigated and work should extend to mixed perovskites and their impact on solar cells.

Supplementary Materials: The following are available online at <http://www.mdpi.com/2079-6412/7/8/115/s1>. Figure S1: SPV spectra of perovskite on molybdenum substrate coated with 0 mg of PMMA in 1 mL of butyl acetate; Figure S2: Grazing incidence X-ray diffraction (GIXRD) pattern for of $\text{CH}_3\text{NH}_3\text{PbI}_3$ on molybdenum substrate coated with 0 mg of PMMA in 1 mL of butyl acetate after storage in air for 50 days; and Figure S3: Tauc gap from SPV and PL spectrum for 40mg/mL of PMMA.

Acknowledgments: C.O. is grateful to the KAAD (Katholischer Akademischer Austauschdienst) for financial support. P.P. is grateful to the Development and Promotion of Science and Technology Talent Project (DPST, Thailand) for financial support. The authors are grateful to M. Lux-Steiner for providing laboratories and for discussions during the beginning of the project at the former Institute of Heterogeneous Materials of the Helmholtz-Zentrum Berlin.

Author Contributions: Conceptualization: Thomas Dittrich and Pongthep Prajontat; Methodology: Pongthep Prajontat, Thomas Dittrich and Celline Awino; Validation: Thomas Dittrich, Pongthep Prajontat and Celline Awino; Formal Analysis: Celline Awino and Thomas Dittrich; Investigation: Celline Awino, Thomas Dittrich and Pongthep Prajontat; Resources: all materials, devices and laboratories were provided by the Helmholtz-Zentrum Berlin; Writing-Original Draft: Celline Awino, Victor Odari and Thomas Sakwa; Writing-Review & Editing: Victor Odari, Thomas Sakwa and Celline Awino; Supervision: Bernd Rech and Thomas Dittrich; Project Administration: Bernd Rech; Funding Acquisition: Celline Awino.

Conflicts of Interest: The authors declare no conflict of interest.

References

- Wolf, S.D.; Holovsky, J.; Moon, S.J.; Löper, P.; Niesen, B.; ledinsky, M.; Haug, F.J.; Yum, J.H.; Balif, C. Organometallic halide perovskites: Sharp optical absorption edge and its relation to photovoltaic performance. *J. Phys. Chem. Lett.* **2014**, *5*, 1035–1039. [[CrossRef](#)] [[PubMed](#)]
- Stranks, S.D.; Eperon, G.E.; Grancini, G.; Menelaou, C.; Alcocer, M.J.P.; Leitens, T.; Herz, L.M.; Petrossza, A.; Snaith, H.J. Electron-hole diffusion lengths exceeding 1 micrometer in an organometal Trihalide perovskite absorber. *Science* **2013**, *342*, 341–344. [[CrossRef](#)] [[PubMed](#)]
- Lee, M.M.; Tauscher, J.; Miyasaka, T.; Murakami, T.N.; Snaith, H.J. Efficient hybrid solar cells based on meso-superstructured orgnaometal halide perovskites. *Science* **2012**, *338*, 643–647. [[CrossRef](#)] [[PubMed](#)]
- Wehrenfennig, C.; Eperon, G.E.; Johnstone, M.B.; Snaith, H.J.; Herz, L.M. High charge carrier mobilities and lifetimes in organolead Trihalide perovskite. *Adv. Mater.* **2014**, *26*, 1584–1589. [[CrossRef](#)] [[PubMed](#)]
- Zhang, L.Q.; Zhang, X.W.; Yin, Z.G.; Jiang, Q.; Liu, X.; Meng, J.H.; Zhao, Y.J.; Wang, H.L. Highly efficient and stable planar heterojunction perovskite solar cells via low temperature solution process. *J. Mater. Chem. A* **2015**, *3*, 12133–12138. [[CrossRef](#)]
- Jeon, J.N.; Noh, H.J.; Yang, S.W.; Kim, C.Y.; Ryu, S.; Seo, J.; Seok, I.S. Compositional engineering of perovskite materials for high-performance solar cells. *Nature* **2015**, *517*, 476–480. [[CrossRef](#)] [[PubMed](#)]
- National Renewable Energy Laboratory (NREL). Best Research-Cell Efficiencies. Available online: <http://www.nrel.gov/ncpv/> (accessed on 26 May 2017).
- Liu, D.; Kelly, T.L. Perovskite solar cells with planar heterojunction structure prepared using room temperature solution processing techniques. *Nat. Photonic* **2014**, *8*, 133–138. [[CrossRef](#)]
- Quan, L.N.; Yuan, M.; Comin, R.; Voznyy, O.; Beauregard, E.M.; Hoogland, S.; Buin, A.; Kirmani, A.R.; Zhao, K.; Amassian, A.; et al. Ligand-stabilized reduced-Dimensionalityperovskites. *J. Am. Chem. Soc.* **2016**, *138*, 2649–2655. [[CrossRef](#)] [[PubMed](#)]
- You, J.; Meng, L.; Song, T.B.; Guo, T.F.; Yang, Y.; Chang, W.-H.; Hong, Z.; Chen, H.; Zhou, H.; De Marco, N.; et al. Improved air stability of perovskite solar cells via solution-processed metal oxide transport layers. *Nat. Nanotechnol.* **2015**, *11*, 75–81. [[CrossRef](#)] [[PubMed](#)]
- Jeon, N.J.; Noh, J.H.; Kim, Y.C.; Yang, W.S.; Ryu, S.; Seok, S.L. Solvent engineering for high performance inorganic-organic hybrid perovskite solar cells. *Nat. Mater.* **2014**, *13*, 897–903. [[CrossRef](#)] [[PubMed](#)]
- Habisreutinger, S.N.; Leijtens, T.; Eperon, G.E.; Stranks, S.D.; Nicholas, R.J.; Snaith, N.H. Carbon nanotube/polymer composite as a highly stable hole collection layer in perovskite solar cells. *Nano Lett.* **2014**, *14*, 5561–5568. [[CrossRef](#)] [[PubMed](#)]
- Song, S.; Hong, W.; Kwon, S.; Lee, T. Passivation effects on ZnO nanowire field effect transistors under oxygen, ambient, and vacuum environments. *Appl. Phys. Lett.* **2008**, *92*, 263109. [[CrossRef](#)]
- Kong, W.; Ding, T.; Bi, G.; Wu, H. Optical characterizations of the surface states in hybrid lead–halide perovskites. *Phys. Chem. Chem. Phys.* **2016**, *18*, 12626–12632. [[CrossRef](#)] [[PubMed](#)]
- Wang, F.; Shimazaki, A.; Yang, F.; Kanahashi, K.; Matsuki, K.; Miyauchi, Y.; Takenobu, T.; Wakamiya, A.; Murata, Y.; Matsuda, K. Highly efficient and stable perovskite solar cells by interfacial engineering using solution-processed polymer layer. *J. Phys. Chem. C* **2017**, *121*, 1562–1568. [[CrossRef](#)]
- Wang, F.; Endo, M.; Mouri, S.; Miyauchi, Y.; Ohno, Y.; Wakamiya, A.; Muratab, B.; Matsuda, K. Highly stable perovskite solar cells with all-carbon hole transport layer. *Nanoscale* **2016**, *8*, 11882–11888. [[CrossRef](#)] [[PubMed](#)]
- Luo, J.; Decoppet, J.; Li, X.; Graetzel, M.; View, B. Polymer-templated nucleation and crystal growth of perovskite films for solar cells with efficiency greater than 21%. *Nat. Energy* **2016**, *1*, 16142. [[CrossRef](#)]
- Dittrich, T.; Awino, C.; Prajontgat, P.; Rech, B.; Lux-Steiner, M.C. Temperature dependence of band gap of $\text{CH}_3\text{NH}_3\text{PbI}_3$ stabalized with PMMA: A modulated surface photovoltage study. *J. Phys. Chem. C* **2015**, *119*, 23968–23972. [[CrossRef](#)]
- Xing, G.; Mathews, N.; Sun, S.; Lim, S.S.; Lam, Y.M.; Grätzel, M.; Mhaisalkar, S.; Sum, T.C. Long-range balanced electron- and hole-transport lengths in organic-inorganic $\text{CH}_3\text{NH}_3\text{PbI}_3$. *Science* **2013**, *342*, 344–347. [[CrossRef](#)] [[PubMed](#)]
- Chan, C.H.; Chen, H.S.; Kao, C.W.; Hsu, H.P.; Huang, Y.S.; Wang, J.S. Surface photovoltage spectroscopy and photoluminescence study of vertically coupled self-assembled InAs/GaAs quantum dot structures. *J. Appl. Phys.* **2006**, *100*, 064301. [[CrossRef](#)]

21. Supasai, T.; Rujisamphan, N.; Ullrich, K.; Chemseddine, A.; Dittrich, T. Formation of a passivating $\text{CH}_3\text{NH}_3\text{PbI}_3/\text{PbI}_2$ interface during moderate heating of $\text{CH}_3\text{NH}_3\text{PbI}_3$ layers. *Appl. Phys. Lett.* **2013**, *103*, 183906. [[CrossRef](#)]
22. Dittrich, T. Principles of Surface Photovoltage (SPV) Techniques and Applications on Solar Cell Materials: An Extended Lecture at HZB. Available online: <http://www.helmholtz-berlin.de/media/media/forschung/energie/heterogen/eta/methods/spv-techniques-2010-08-09.pdf> (accessed on 5 June 2013).
23. Goodmann, A.M. A method for the measurement of short minority carrier diffusion lengths in semiconductors. *J. Appl. Phys.* **1961**, *32*, 2550–2552. [[CrossRef](#)]
24. Prajongtat, P.; Dittrich, T. Precipitation of $\text{CH}_3\text{NH}_3\text{PbCl}_3$ in $\text{CH}_3\text{NH}_3\text{PbI}_3$ and its impact on modulated charge separation. *J. Phys. Chem. C* **2015**, *119*, 9926–9933.
25. Yu, H.; Wang, F.; Xie, F.; Li, W.; Chen, J.; Zhao, N. The role of chlorine in the formation process of “ $\text{CH}_3\text{NH}_3\text{PbI}_{3-x}\text{Cl}_x$ ” Perovskite. *Adv. Funct. Mater.* **2014**, *24*, 7102–7108. [[CrossRef](#)]
26. Lin, X.Z.; Dittrich, T.; Fengler, S.; Lux-Steiner, M.C.; Ennaoui, A. Correlation between processing conditions of $\text{Cu}_2\text{ZnSn}(\text{S}_x\text{Se}_{1-x})_4$ and modulated surface photovoltage. *Appl. Phys. Lett.* **2013**, *102*, 143903. [[CrossRef](#)]
27. Tauc, J. Optical properties & electronic structure of amorphous Ge and Si. *Mater. Res. Bull.* **1968**, *3*, 37–46.
28. Bretschneider, S.A.; Weickert, J.; Dorman, J.A.; schmidt-Mende, L. Research Update: Physical and electrical characteristics of lead halide perovskites for solar cell applications. *APL Mater.* **2014**, *2*, 040701. [[CrossRef](#)]
29. Naikaew, P.; Prajongtat, P.; Dittrich, T.; Lux-Steiner, M.C. Role of phase composition for electronic states in $\text{CH}_3\text{NH}_3\text{PbI}_3$ prepared from $\text{CH}_3\text{NH}_3\text{I}/\text{PbCl}_2$ solution. *Appl. Phys. Lett.* **2015**, *106*, 232104. [[CrossRef](#)]
30. Barugkin, C.; Cong, J.; Duong, T.; Rahman, S.; Nguyen, H.T.; Macdonald, D.; White, T.P.; Catchpole, K.R. Ultralow absorption coefficient and temperature dependence of radiative recombination of $\text{CH}_3\text{NH}_3\text{PbI}_3$ perovskite from photoluminescence. *J. Phys. Chem. Lett.* **2015**, *6*, 767–772. [[CrossRef](#)] [[PubMed](#)]
31. Wang, Z.Q.; Zhang, Z.B.; Zhang, M.H. The efficient synthesis of a molybdenum carbide catalyst via H_2 -thermal treatment of a Mo (V1)-hexamethylenetetramine complex. *Dalton Trans.* **2011**, *40*, 1098–1104. [[CrossRef](#)] [[PubMed](#)]
32. Kojima, A.; Teshima, K.; Shirai, Y.; Miyasaka, T. Organometal halide perovskites as visible-light sensitizers for photovoltaic cells organometal halide perovskites as visible-light sensitizers for photovoltaic. *J. Am. Chem. Soc.* **2009**, *131*, 6050–6051. [[CrossRef](#)] [[PubMed](#)]
33. Fu, K.; Lim, S.S.; Fang, Y.; Boix, P.P.; Mathews, N.; Sum, T.C.; Wonig, L.H.; Mhaisalkar, S. Modulating $\text{CH}_3\text{NH}_3\text{PbI}_3$ perovskite crystallization behavior through precursor concentration. *Nano Brief Rep. Rev.* **2014**, *9*, 1440003. [[CrossRef](#)]
34. Sun, S.; Salim, T.; Mathews, N.; Duchamp, M.; Boothroyd, C.; Xing, G.; Sum, T.C.; Lam, Y.M. The origin of high efficiency in low temperature solution-processable bilayer organometal halide hybrid solar cells. *Energy Environ. Sci.* **2014**, *7*, 399–407. [[CrossRef](#)]



© 2017 by the authors. Licensee MDPI, Basel, Switzerland. This article is an open access article distributed under the terms and conditions of the Creative Commons Attribution (CC BY) license (<http://creativecommons.org/licenses/by/4.0/>).